Preprints of the 21st IFAC World Congress (Virtual)
Berlin, Germany, July 12-17, 2020

Two Degrees of Freedom Slip Controller with Lateral Torque Distribution ⋆

Wolfgang Degel [*,**] **Stefan Lupberger** [*,**] **Dirk Odenthal** [*]
Naim Bajcinca [**]

[*] *BMW M GmbH, 85748 Garching near Munich, Germany (e-mail: wolfgang.wd.degel@bmw-m.com, stefan.lupberger@bmw-m.com, dirk.odenthal@bmw-m.com)*
[**] *University of Kaiserslautern, Chair of Mechatronics in Mechanical and Automotive Engineering, 67663 Kaiserslautern Germany (e-mail: naim.bajcinca@mv.uni-kl.de)*

Abstract: Current slip control systems focus on vehicles with single-axle drive or all-wheel drive. This work presents a new two degrees of freedom slip controller affecting the average wheel speed and the wheel speed difference between the left and right wheel of a driven axle. The approach is applicable for electronically controlled limited-slip differentials and individually controllable brake actuators. The control design is performed with input-output linearization and global stability in the sense of Lyapunov is proven for the zero dynamics. The proposed control system is evaluated in a prototype vehicle and fulfills the task of traction control.

Keywords: Automotive control, slip control, input-ouptut linearization, stability of nonlinear systems, limited-slip differential, brake control.

1. INTRODUCTION

Traction Control Systems (TCSs) are necessary to prevent the driven wheels from spinning and enable acceleration on slippery surfaces. They control the friction forces between tires and road and are an important control system as they contribute to increased vehicle stability, drivability, and performance of ground vehicles (van Zanten et al. (1995)). The first TCSs were introduced in the 90s and developed over the past decades (e.g. Rittmannsberger (1988)). Due to the faster dynamics of electric motors as well as the enhanced power of modern turbo charged combustion engines further improvements of TCSs are necessary (Ivanov et al. (2015)).

The majority of literature concerns slip or wheel speed control for a vehicle with front-wheel, rear-wheel, or all-wheel drive (Ivanov et al. (2015)). Furthermore, lateral torque distribution increase the overall traction during dynamic cornering as well as take off or acceleration on different road frictions for the left and right wheel (μ-split). For such driving maneuvers electronically controlled limited-slip differentials (eLSD) and individually controllable brake actuators generate a torque distribution for the driven wheels. Depending on the hardware setup and limitiations of the vehicle both actuator concepts are used alternatively and complementary for improved traction. Additionally, torque vectoring affects the yaw rate, which can be used by Yaw Stability Control (YSC).

Resta et al. (2005) and Cheli et al. (2005) present a combination of feedforward and proportional-integral (PI) controller to determine the lateral torque distribution at the rear axle. The approach is evaluated in simulative and experimental tests for an semi-active differential. Instead, Marino and Scalzi (2008) use a Lyapunov-based control design for the same vehicle setup. Isermann (2006) presents a two degrees of freedom traction controller. The speed of the cardan shaft is controlled by the engine and two brakes, while the wheel speed difference is controlled by the difference between the left and right brake torque. Hosomi et al. (2000) use simultaneously control of the throttle and all four brakes for increased traction during μ-split driving situations.

However, the concepts are limited to either eLSD or brakes and the dynamics of the powertrain or actuators are often neglected. For ideal traction during dynamic cornering and μ-split driving, simultaneous control of the average wheel speed and wheel speed difference of the left and right is necessary. Furthermore, eLSD and brake actuators should be considered for lateral torque distribution to enable alternatively and complementary control for both actuators. Therefore, we present a new two degrees of freedom slip controller based on input-output-linearization. The approach regards both actuators and extends our previous work for vehicles with two-wheel drive (2WD) by Reichensdörfer et al. (2018), Reichensdörfer et al. (2020), Zech et al. (2017), Zech et al. (2018), and four-wheel drive (4WD) by Reichensdörfer et al. (2019).

This paper is organized as follows. At first, an unified vehicle model is described in Section 2. Section 3 discusses the control design using input-output-lineariziation and the proof of stability for the zero dynamics. After that, experimental results are shown for a prototype vehicle with rear-wheel drive in Section 4. Finally, a short conclusion is given in Section 5.

⋆ This work was supported by BMW M GmbH.

2. SYSTEM DESCRIPTION

The vehicle model is used for control design and proof of stability. Fig. 1 shows two schematic powertrains usable for vehicles with front-wheel or rear-wheel drive. Note that the non-driven axle is not shown in Fig. 1. The vehicle on the left-hand side is equipped with an eLSD which enables lateral torque distribution. A detailed description of possible hardware setups is given e.g. by Hancock et al. (2007). The vehicle on the right-hand side uses brake actuators for torque vectoring. The dynamic behaviour of the actuators and powertrain is described by the following equations:

$$\tau_m \dot{T}_m = T_{m,d} - T_m \,, \tag{1a}$$
$$\tau_e \dot{T}_e = T_{e,d} - T_e \,, \tag{1b}$$
$$\tau_{br,j} \dot{T}_{br,j} = T_{br,j,d} - T_{br,j} \,, \tag{1c}$$
$$\Delta\dot{\phi} = \omega_c / i_G - (\omega_{w,l} + \omega_{w,r})/2 \,, \tag{1d}$$
$$J_c \dot{\omega}_c = T_m - 2\,T_w / i_G \,, \tag{1e}$$
$$(J_w/2)\,\dot{\omega}_{w,j} = T_w - r_w F_{x,j} + T_j \,, \tag{1f}$$
$$T_w = k_c \Delta\phi + d_c \Delta\dot{\phi} \,. \tag{1g}$$

The index $j \in \{l,\, r\}$ denotes the left or right wheel. The first actuator (index m) represents a central motor like a combustion engine or electric motor and generates a drive torque T_m. The equations (1b), (1c) represent the eLSD (index e) and the brake actuators (index br). All actuator dynamics are approximated as first-order lags with time constants τ_m, τ_e, $\tau_{br,j}$, actual torques T_m, T_e, $T_{br,j}$, and desired torques $T_{m,d}$, $T_{e,d}$, $T_{br,j,d}$.

The gear ratio $i_G = i_a i_d$ contains the ratio of the automatic transmission i_a and differential i_d. The derivative of the twist angle $\Delta\dot{\phi}$ describes the difference between the rotational speed of the crankshaft ω_c and the average speed of the left and right wheel $\omega_{w,j}$. Additionally, J_c is the inertia of the crankshaft, J_w is the inertia for both wheels, and r_w denotes the tire radius. The cardan shaft between gearbox and wheels is modelled as a torsion spring with torsional stiffness k_c and damping coefficient d_c. For synthesis, both drive shafts are assumed to be rigid. The torque for one wheel is denoted by T_w, the friction force between tire and road by $F_{x,j}$. The wheel dynamics are affected by an additional torque T_j depending on the used powertrain. Considering forward motion $\omega_{w,j} > 0$ and a vehicle with

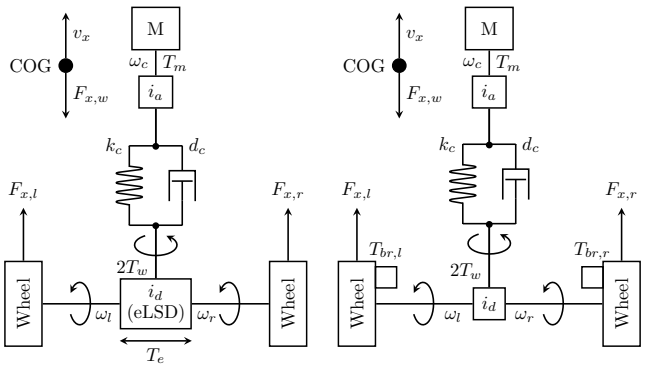

Fig. 1. Schematic powertrain for a driven axle with an eLSD (left-hand side) and with two brake actuators (right-hand side).

an eLSD, the torques are set to $T_r = -T_l = T_e/2$. In case of two brake actuators, the relation $T_j = T_{br,j} \leq 0$ is used.

However, the introduced system (1a)-(1g) has a few disadvantages. The wheel dynamics (1f) are coupled since both depend on the drive torque T_w. In case of two brake actuators there are three inputs $\boldsymbol{u} = [T_{m,d}\ T_{br,l}\ T_{br,r}]^T \in \mathbb{R}^3$ which are controlling three speeds $\boldsymbol{y} = [\omega_c\ \omega_{w,l}\ \omega_{w,r}]^T \in \mathbb{R}^3$. Besides, in case of an eLSD, the torques $T_r = -T_l = T_e/2$ are conditional and both wheel speeds $w_{w,j}$ depend on just one actuator. To unify both concepts we introduce a similar transformation to Isermann (2006). The average wheel speed $\omega_w = (\omega_r + \omega_l)/2$ and wheel speed difference $\Delta\omega_w = \omega_r - \omega_l$ describe the wheel dynamics in the sense of degrees of freedom:

$$J_w \dot{\omega}_w = 2\,T_w - r_w (F_{x,r} + F_{x,l}) \,, \tag{2a}$$
$$(J_w/2) \Delta\dot{\omega}_w = T_d - r_w (F_{x,r} - F_{x,l}) \,. \tag{2b}$$

The equations (2a) and (2b) are decoupled, since the average speed ω_w only depends on drive torque T_w. The wheel speed difference $\Delta\omega_w$ is only affected by the differential torque T_d which depends on the powertrain:

$$\tau_d \dot{T}_d = T_{d,d} - T_d \,, \tag{3a}$$
$$T_{d,d} = \begin{cases} T_{e,d} & \text{using eLSD} \,, \\ T_{br,r,d} - T_{br,l,d} & \text{using brakes} \,. \end{cases} \tag{3b}$$

Remark 1. In case of brake actuators, the equations are coupled since the brake torques reduce the average wheel speed ω_w. For simplification, it is assumed that the drive torque T_m compensates the amount of brake torque and the effect can be neglected.

The friction forces $F_{x,j}$ between tires and road are depicted by the following model introduced by Pacejka (2012):

$$F_{x,j} = \mu_j F_{z,j} \sin(C_p \arctan(B_p \lambda_j)) \,, \tag{4a}$$
$$F_{z,l} = (F_{z,n}/2)\, k_x\, (1 - k_y) \,, \tag{4b}$$
$$F_{z,r} = (F_{z,n}/2)\, k_x\, (1 + k_y) \,, \tag{4c}$$
$$F_{z,n} = mg(l_{fa} + l_{ra} - l_k)/(l_{fa} + l_{ra}), \tag{4d}$$
$$\lambda_l = (\omega_l r_w - v_x)/\max_\epsilon(|\omega_l r_w|_\epsilon, |v_x|_\epsilon) \,, \tag{4e}$$
$$\lambda_r = (\omega_r r_w - v_x)/\max_\epsilon(|\omega_r r_w|_\epsilon, |v_x|_\epsilon) \,. \tag{4f}$$

The tire model includes the stiffness B_p, shape factor C_p, different road frictions $\mu_j \in (0,\, \mu_{max}]$, as well as different wheel loads $F_{z,j}$. Further, $F_{z,n}$ is the nominal wheel load including m as total vehicle mass, g as gravitational constant, l_{fa} and l_{ra} as distances between the center of gravity (COG) and the front and rear axle, respictively. The index $k \in \{fa,\, ra\}$ depicts front-wheel or rear-wheel drive. The scaling factor $k_x \in [0, mg/F_{z,n}]$ denotes the wheel load shift through longitudinal acceleration. At the minimal load shift $k_x = 0$ the axle is fully lifted, while at the maximal load shift $k_x = m\,g/F_{z,n}$ the entire wheel load is distributed between both wheels. The parameter $k_y \in [-1,\, 1]$ denotes the wheel load shift through lateral accelerations like in turning maneuvers. The left tire and the right tire are fully lifted for $k_y = 1$ and $k_y = -1$, respectively.

Remark 2. Both scaling factors k_x, k_y depend on the acceleration of the vehicle and are dynamic states. However, they are modelled as varying parameters. This simplification is valid since the wheel dynamic changes much faster than the vehicle dynamics (van Zanten et al. (1995)).

The longitudinal slip λ_j is defined similiar to Reichensdörfer et al. (2018), whereby the rotational speeds for the left and right wheel are $\omega_l = \omega_w - \Delta\omega_w/2$ and $\omega_r = \omega_w + \Delta\omega_w/2$, respectively. The functions $\max_\epsilon(a,b) := (1/2)(a+b+|a-b|_\epsilon)$ and $|a|_\epsilon := \sqrt{a^2+\epsilon}$ are applied to avoid the singularity of the denominator. Finally, the following equations describe the vehicle motion in longitudinal direction:

$$m\dot{v}_x = F_{x,l} + F_{x,r} - F_{x,w} \,, \tag{5a}$$
$$F_{x,w} = (1/2)\rho c_w A_{fs} v_x |v_x| \,. \tag{5b}$$

Here, $F_{x,w}$ is the aerodynamic drag force in longitudinal direction, ρ the air density, c_w the aerodynamic drag coefficient, and A_{fs} the vehicle front surface. All vehicle parameters are physically motivated and therefore strictly positive and finite. Besides, the shape factor $C_p \in (1,2)$ is limited through physically motivation (Pacejka (2012)).

The vehicle dynamics are described in state-space notation by $\dot{\boldsymbol{x}} = \boldsymbol{f}(\boldsymbol{x},\boldsymbol{u})$, $\boldsymbol{y} = \boldsymbol{h}(\boldsymbol{x})$ with the state vector $\boldsymbol{x} = [T_m \; T_d \; \Delta\phi \; \omega_c \; \omega_w \; \Delta\omega_w \; v_x]^T \in \mathbb{R}^7$ and the input vector $\boldsymbol{u} = [T_{m,d} \; T_{d,d}]^T \in \mathbb{R}^2$. The output vector $\boldsymbol{y} = [x_4/i_G \; x_6]^T \in \mathbb{R}^2$ contains the rotational speed of the crankshaft normalized to the wheels and the wheel speed difference. The remaining vectors are described as follows:

$$\boldsymbol{f}(\boldsymbol{x},\boldsymbol{u}) = \begin{bmatrix} (u_1 - x_1)/\tau_m \\ (u_2 - x_2)/\tau_d \\ x_4/i_G - x_5 \\ (x_1 - 2\,T_w/i_G)/J_c \\ (2\,T_w - r_w(F_{x,r} + F_{x,l}))/J_w \\ (x_2 - r_w(F_{x,r} - F_{x,l}))/(J_w/2) \\ (F_{x,l} + F_{x,r} - F_{x,w})/m \end{bmatrix} . \tag{6}$$

The nonlinear system (6) extends previous work for the 2WD case by Reichensdörfer et al. (2018) and Zech et al. (2018) to 7 states, 2 inputs, and 2 outputs. Furthermore, the tire forces $F_{x,j}$, road frictions μ_j and wheel loads $F_{z,j}$ are considered separately for the left and right wheel.

3. CONTROL DESIGN AND ANALYSIS

At first, the control design using the method of Input-Output-Linearization (IOL), first introduced by Isidori (1989), is performed. Afterwards, the proof of stability is shown and the overall control structure is presented.

3.1 Control Design with Input-Output-Linearization

The control laws are obtained by deriving each output. The derivatives of the first output $y_1 = x_4/i_G$ are

$$\dot{y}_1 = \frac{1}{i_G J_c}\Big(x_1 - \frac{2}{i_G}\Big(k_c x_3 + d_c\Big(\frac{x_4}{i_G} - x_5\Big)\Big)\Big) \,, \tag{7a}$$
$$\ddot{y}_1 = \frac{1}{i_G J_c}\Big(\frac{u_1 - x_1}{\tau_m} - \frac{2}{i_G}\Big(k_c \dot{x}_3 + d_c\Big(\frac{\dot{x}_4}{i_G} - \dot{x}_5\Big)\Big)\Big) \,. \tag{7b}$$

Deriving the second output $y_2 = x_6$ result in:

$$\dot{y}_2 = \frac{2}{J_w}(x_2 - r_w(F_{x,r} - F_{x,l})) \,, \tag{8a}$$
$$\ddot{y}_2 = \frac{2}{J_w}\Big(\frac{u_2 - x_2}{\tau_d} - r_w(\dot{F}_{x,r} - \dot{F}_{x,l})\Big) \,. \tag{8b}$$

Defining $v_{1,2} := \ddot{y}_{1,2}$, the control laws are as follows:

$$u_1 = x_1 + J_c \tau_m i_G v_1 + \frac{2\tau_m}{i_G}\Big(k_c \dot{x}_3 + d_c\Big(\frac{\dot{x}_4}{i_G} - \dot{x}_5\Big)\Big) \tag{9a}$$
$$u_2 = x_2 + (J_w/2)\tau_d v_2 + r_w \tau_d (\dot{F}_{x,r} - \dot{F}_{x,l}) \,. \tag{9b}$$

The control laws are decoupled since u_1 only contains v_1 and u_2 only contains v_2. This allows a realization on different control units which is an advantage for vehicles with a networked hardware setup. The specific implementation in a protoype vehicle is described in section 3.3.

3.2 Zero Dynamics and Stability Analysis

The relative degree of the system is $r = 4$, consequently the internal dynamics are of third degree. To analyze the zero dynamics, the system is transformed into Byrnes-Isidori normal form (Byrnes and Isidori (1989)). The state transformation $\boldsymbol{\xi} = \boldsymbol{\varphi}(\boldsymbol{x})$ is defined by $\boldsymbol{\xi} = [y_1 \; \dot{y}_1 \; y_2 \; \dot{y}_2 \; x_3 \; x_5 \; x_7]^T \in \mathbb{R}^7$. This is a global diffeomorphism since $\det(\partial\boldsymbol{\varphi}(\boldsymbol{x})/(\partial\boldsymbol{x})) = 2/(J_c J_w i_G^2) \neq 0, \forall \boldsymbol{x}$. Consider the inverse transformation $\boldsymbol{x} = \boldsymbol{\varphi}^{-1}(\boldsymbol{\xi})$, the control laws (9a),(9b), and setting $\xi_1 = \xi_2 = \xi_3 = \xi_4 = v_1 = v_2 = 0$, the zero dynamics are given by

$$\begin{bmatrix} \dot{z}_1 \\ \dot{z}_2 \\ \dot{z}_3 \end{bmatrix} = \begin{bmatrix} -z_2 \\ (2(k_c z_1 - d_c z_2) - r_w(F_{x,l} + F_{x,r}))/J_w \\ (F_{x,l} + F_{x,r} - F_{x,w})/m \end{bmatrix} . \tag{10}$$

The vector $\boldsymbol{z}$ is defined by $\boldsymbol{z} = [z_1 \; z_2 \; z_3]^T = [\xi_5 \; \xi_6 \; \xi_7]^T = [\Delta\phi \; \omega_w \; v_x]^T$. Consider $y_2 = \Delta\omega_w = 0$, the wheel slips of both tires are equal and depend on the wheel speed z_2:

$$\overline{\lambda} := \lambda_l = \lambda_r = \frac{z_2 r_w - z_3}{\max_\epsilon(|z_2 r_w|_\epsilon, |z_3|_\epsilon)} \,. \tag{11a}$$

This simplifies the tire forces $F_{x,j}$ as follows:

$$\overline{F}_x := F_{x,l} + F_{x,r} = \overline{\mu}\,\overline{F}_z \sin(C_p \arctan(B_p \overline{\lambda})) \,, \tag{12a}$$
$$\overline{\mu} := (\mu_l(1 - k_y) + \mu_r(1 + k_y))/2 \,, \tag{12b}$$
$$\overline{F}_z := \overline{m}\, g(l_{fa} + l_{ra} - l_k)/(l_{fa} + l_{ra}) \,. \tag{12c}$$

Consider $k_y \in [-1,1]$, the term $\overline{\mu}$ is interpreted as a weighted average road friction. The expression $\overline{F}_z$ denotes the wheel load of the axle with the scaled vehicle mass $\overline{m} = k_x m \geq 0$. The zero dynamics result in

$$\begin{bmatrix} \dot{z}_1 \\ \dot{z}_2 \\ \dot{z}_3 \end{bmatrix} = \begin{bmatrix} -z_2 \\ (2(k_c z_1 - d_c z_2) - r_w \overline{F}_x)/J_w \\ (\overline{F}_x - F_{x,w})/m \end{bmatrix} . \tag{13}$$

The system (13) is similar to the zero dynamics used by Reichensdörfer et al. (2018). The main deviation is the definition of the tire force $\overline{F}_x$. Reichensdörfer et al. (2018) defined their road friction by $\mu \in (0, \mu_{max}]$ and used a constant wheel load F_z. In equation (12b), the road friction is a linear function with respect to k_y and limited to μ_l and μ_r. Since $\overline{\mu} \in [\mu_l, \mu_r] \in (0, \mu_{max}]$ applies, the weighted average road friction $\overline{\mu}$ has not be considered additionally. The wheel load in equation (12c) varies with the vehicle mass $\overline{m} = k_x m \in [0, m^2 g/F_{z,n}]$. In the case of $\overline{m} > 0$, the zero dynamics are equal and the proof of stability by Reichensdörfer et al. (2018) is applied. The case $\overline{m} = 0 \Rightarrow \overline{F}_x = 0$ reduces the zero dynamics (13) to

$$\begin{bmatrix} \dot{z}_1 \\ \dot{z}_2 \\ \dot{z}_3 \end{bmatrix} = \begin{bmatrix} -z_2 \\ 2(k_c z_1 - d_c z_2)/J_w \\ -F_{x,w}/m \end{bmatrix} \tag{14}$$

and stability has to be proved. At first the equilibrium of the zero dynamics (14) is determined. Then, the definiteness of the Lyapunov function of Reichensdörfer et al. (2018) is verified for $\overline{m} = 0 \Rightarrow \overline{F}_x = 0$.

Lemma 1. The zero dynamics (14) have a unique equilibrium $\boldsymbol{z}^* = \mathbf{0}$.

Proof. From (14), it is clear that $\dot{z}_1 = z_2 = 0$ and consequently $\dot{z}_2 = z_1 = 0$. The last equation $F_{x,w} = 0$ is only satisfied for $z_3 = 0$. This leads to the unique equilibrium $\boldsymbol{z}^* = \mathbf{0}$. □

Theorem 1. Consider $\overline{m} = 0$, the Lyapunov function

$$\begin{aligned} V(\boldsymbol{z}) = \boldsymbol{z}^T \boldsymbol{P} \boldsymbol{z} = \boldsymbol{z}^T \begin{bmatrix} p_{11} & -1/2 & 0 \\ -1/2 & p_{22} & 0 \\ 0 & 0 & p_{33} \end{bmatrix} \boldsymbol{z} = \\ = p_{11} z_1^2 + p_{22} z_2^2 + p_{33} z_3^2 - z_1 z_2 \,, \\ p_{11} = (2k_c/J_w)\, p_{22} + d_c/J_w > 0 \,, \\ p_{22} = \alpha + 2J_w/d_c > 0 \,, \\ p_{33} = (m/J_w)\, p_{22} > 0 \,, \\ \alpha = (\bar{c}_x r_w^2)/(24 k_c \sqrt{\epsilon}) \geq 0 \end{aligned} \tag{15}$$

introduced by Reichensdörfer et al. (2018) is still a valid candidate for the zero dynamics (14).

Proof. The coefficients from (15) contain the longitudinal slip stiffness $\bar{c}_x$ denoting the slope of the tire force $\overline{F}_x$ at the origin ($\overline{\lambda} = 0$):

$$\bar{c}_x := \frac{d}{d\overline{\lambda}} \overline{F}_x \bigg|_{\overline{\lambda}=0} = \overline{\mu}\, \overline{F}_z B_p C_p \geq 0 \,. \tag{16}$$

In the case of $\overline{m} = \overline{F}_z = 0 \Rightarrow \bar{c}_x = 0$ and therefore $\alpha = 0$. The matrix $\boldsymbol{P} = \boldsymbol{P}^T$ is symmetric and contains the mixed term $z_1 z_2$. To analyze the definiteness of the Lyapunov function we use Sylvester's criterion. The matrix $\boldsymbol{P}$ is positive definite if all principal minors are positive (Gilbert (1991)). Since $p_{11} > 0$ and z_3 is only included in term $p_{33} z_3^2$, it is sufficient to show $p_{11} p_{22} - 1/4 > 0$. Consider $\alpha = 0$, this leads to $8 k_c J_w / d_c^2 + 2 > 1/4$ which is guaranteed for all possible combinations of vehicle parameters. Even with the mixed term $z_1 z_2$, the Lyapunov function $V(\boldsymbol{z})$ is a valid candidate. □

Theorem 2. Consider $\alpha = 0$, the time derivative of the Lyapunov function

$$\dot{V}(\boldsymbol{z}) = -(2k_c/J_w) z_1^2 - 7 z_2^2 - (2 A_{fs} c_w \rho / d_c) z_3^2 |z_3| \tag{17}$$

is negative definite for all vehicle parameters:

Proof. The function $\dot{V}(\boldsymbol{z})$ is quadratic in $\boldsymbol{z}$ and all vehicle parameters in (17) are strictly positive. Consequently, $\dot{V}(\boldsymbol{z})$ is negative definite and the unique equilibrium $\boldsymbol{z}^*$ located at the origin of the zero dynamics (14) is uniformly globally asymptotically stable in the sense of Lyapunov. The scope of application of the Lyapunov function (15) is extended to zero dynamics regarding different road frictions μ_j and wheel loads $F_{z,j}$. □

3.3 Control Structure

The structure for the proposed control design is depicted in Fig. 2. The control laws (9a) - (9b) include the twist angle $x_2 = \Delta\phi$, the road friction μ_j, and the tire parameters B_p, C_p. These variables are uncertain in a modern vehicle and can not be used directly. For the implementation of the first control law (9a), we use similar to previous work, two separate filters $F(s) = s/(\tau_F s + 1)$ for the approximation of $\dot{x}_4$, $\dot{x}_5$. The second control law (9b) requires the derivatives of the tire forces $\dot{F}_{x,j}$ which are

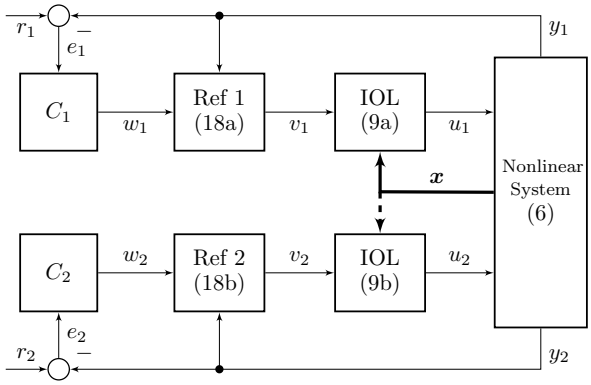

Fig. 2. Control structure for the closed-loop system.

uncertain as well. However, the goal of the control system is to track a slowly varying reference slip. Therefore, $\lambda_j \approx \text{const.} \Rightarrow F_{x,j} \approx \text{const.}$ and consequently $\dot{F}_{x,j} \approx 0$ is obtained. The neglection of the $\dot{F}_{x,j}$ term is symbolized by the dashed line in Fig. 2. The states x_1, x_2, x_4, x_5 can be measured whereas the remaining physical parameters in (9a),(9b) are well-known from CAD models or can be obtained by system identification (Zech et al. (2018)). Therefore, the control laws are able to be implemented in a prototype vehicle.

The control laws (9a) - (9b) include the inputs $v_{1,2}$ which are described by the reference dynamics as a linear integral element with first-oder lag and new inputs $w_{1,2}$:

$$v_1 = (i_G/(\tau_m J_w)) w_1 - (1/\tau_m) \dot{y}_1, \tag{18a}$$
$$v_2 = (2 i_G/(\tau_d J_w)) w_2 - (1/\tau_d) \dot{y}_2, \,. \tag{18b}$$

Furthermore, two linear controllers $C_{1,2}$ are used for compensation of model uncertainties and disturbances. In this work, we use proportional-integral-derivative (PID) controllers regarding actuator saturations by an anti-windup. Both controllers are tuned experimentally to achieve tracking and robustness for varying driving conditions as well as different road frictions. The reference speeds r_1, r_2 are generated from a superimposed controller considering the current driving situation including lateral dynamics, road friction as well as over- and understeering. Additionally, the reference speeds can be used by YSC for increased stability. The first controller is activated similarly to standard TCSs described by e.g. Chen et al. (2012). If the actual wheel speed y_1 exceeds the reference speed r_1, the driver input is overwritten. The second reference speed consists of an upper and lower threshold $r_{2,\max/\min}$. If the speed difference exceeds one of the thresholds, the controller is activated and the following control error is used:

$$e_2 = \begin{cases} r_{2,\max} - y_2, & \text{if } y_2 \geq 0 \,, \\ r_{2,\min} - y_2, & \text{if } y_2 < 0 \,. \end{cases} \tag{19}$$

Remark 3. Consider $y_2 = \omega_r - \omega_l \gg 0$, the right wheel is spinning much faster than the left wheel. Therefore, the upper threshold $r_{2,\max}$ is used, the control error e_2 is negative and consequently, a negative transfer torque is applied to the controller u_2. In case of an eLSD ($T_r = -T_l = T_e/2 < 0$), the drive torque is vectored to the left wheel. In case of two brakes ($T_{br,r} - T_{br,l} < 0$, $T_{br,j} \leq 0$) the right brake is used. In both cases the spinning of the right wheel is reduced and the overall traction is improved. The case $y_2 \ll 0$ follows analogously.

4. EXPERIMENTAL RESULTS

4.1 Implementation Details

The evaluation of the approach is investigated in a prototype vehicle with rear-wheel drive. A combustion engine provides drive torque T_m to the rear axle which is distributed by an active limited-slip differential (ALSD). The ALSD includes an electric motor that acts on a clutch pack coupling the differential box and one drive shaft. Since differential torque is always transferred from the faster to the slower wheel, the ALSD is able to control the magnitude of differential torque but not its direction (Ivanović et al. (2012), Piyabongkarn et al. (2006)). The first controller u_1 is implemented on the engine control unit (ECU, 10 ms task). The second controller u_2 and the reference speed computation, are implemented on a driving dynamics control unit (DCU, 5 ms task). The distribution of both controllers is required since the used test vehicle has a networked hardware setup.

The values of the vehicle parameters assumed in this paper are $\tau_m = \tau_e = 0.02\,\mathrm{s}$, $i_G = 10$, $J_c = 0.23\,\mathrm{kg\,m^2}$, $J_w = 5\,\mathrm{kg\,m^2}$, $r_w = 0.33\,\mathrm{m}$, $B_p = 10.3$, $C_p = 1.8$, $k_c = 5300\,\mathrm{Nm/rad}$, $d_c = 15\,\mathrm{Nm\,s/rad}$, $m = 2000\,\mathrm{kg}$, $g = 9.81\,\mathrm{m/s^2}$, $l_{fa} = 1.3\,\mathrm{m}$, $l_{ra} = 1.4\,\mathrm{m}$, $\rho = 1.1\,\mathrm{kg/m^3}$, $c_w = 0.3$, $A_{fs} = 2.4\,\mathrm{m^2}$.

4.2 Experimental Evaluation

The experiments are performed during driving through a right corner on dry asphalt ($\mu_j = 1$) to show improved cornering traction. The results are shown in Fig. 3. The vehicle accelerates under full throttle which requires reduction of drive torque T_m. Besides, the cornering results in high lateral acceleration which causes the inner right wheel to spin. The ALSD distributes the torque to the outer left wheel. The first controller u_1 is activated at $t = 0.5\,s$ (visualized by the shaded area), while at $t = 0.9\,s$, the second controller u_2 is additionally activated (visualized by the vertical line). In Fig. 3a, the wheel speed y_1 is controlled as soon as it exceeds the reference speed r_1. Fig. 3b depicts the control of the wheel speed difference y_2. After activation, the reference wheel speed difference r_2 decreases to zero. Consider the vehicle speed v_x and equations (4e) - (4f), the wheel speeds can be transformed to the average slip value $\lambda = (\lambda_r + \lambda_l)/2$ and slip difference $\Delta\lambda = \lambda_r - \lambda_l$ shown in Fig. 3c. Fig. 3d displays the differential torque T_e and the resulting wheel torques $T_{\triangle,j}$.

The control system is able to improve the traction of the vehicle. During the maneuver described in Fig. 3, the vehicle accelerates with $a_x = 2.4\,m/s^2$ and $a_y = 9\,m/s^2$ in longitudinal and lateral direction. The same maneuver performed without the second controller u_2 achieves the same lateral acceleration but only a longitudinal acceleration of $a_x = 1.5\,m/s^2$. The overall traction of the vehicle is improved during accelerated cornering.

However, there are significant oscillations for the measured wheel speed difference y_2 (Fig. 3b). These are caused by the nonlinear tire-road contact and are additionally strengthened by the coupling of both drive shafts (Rosenberger et al. (2012)). Due to the low actuator dynamic τ_e, it is not possible to damp these oscillations sufficiently. Nevertheless, the filtered wheel speed difference $y_{2,\mathrm{filt}}$ is able

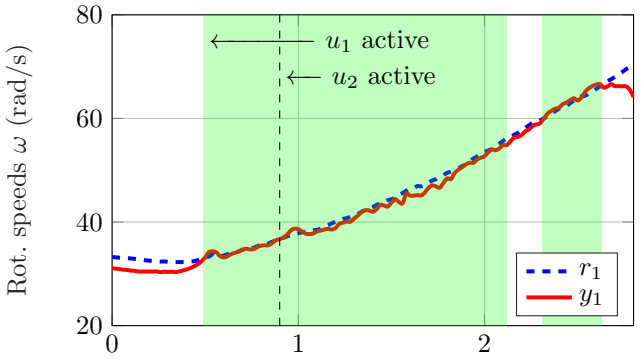

(a) Reference tracking of r_1 during dynamic cornering.

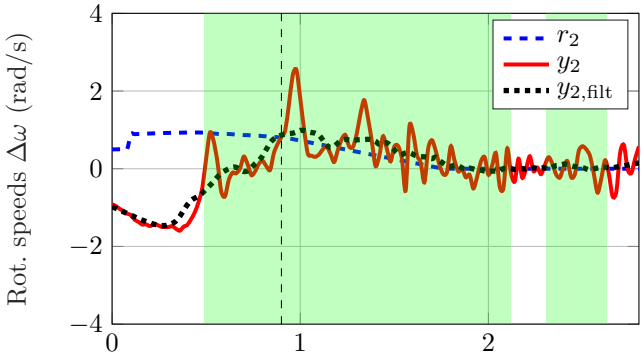

(b) Reference tracking of r_2 during dynamic cornering.

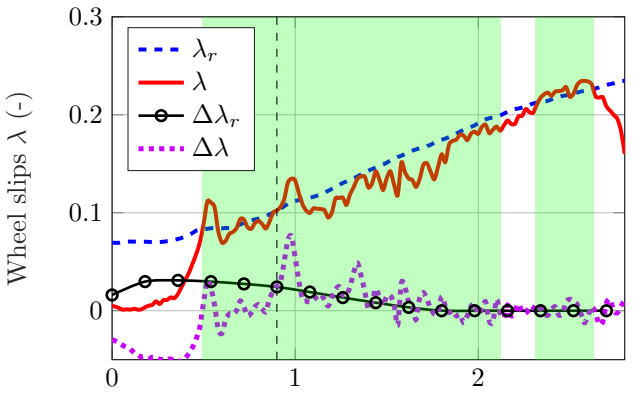

(c) Reference tracking with continuously increasing target slip λ_r and decreasing target difference slip $\Delta\lambda_r$.

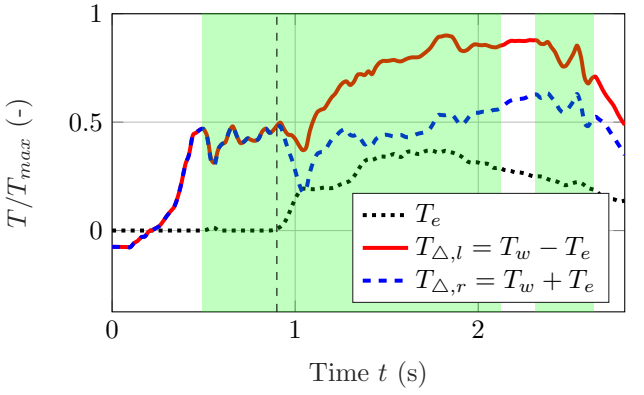

(d) Normalized differential torque T_e and wheel torques $T_{\triangle,j}$.

Fig. 3. Dynamic cornering on dry asphalt (active u_1 shaded).

to follow the reference speed r_2. The approach could be investigated in simulation with an ideal actuator. Furthermore, it is feasible to apply the concept to a vehicle with two electric motors instead of a mechanical differential. Such powertrains can provide torque vectoring with higher dynamics than eLSD or brake actuators (de Castro et al. (2007), Vitols and Galkin (2012)).

5. CONCLUSION

This work extended the average wheel speed control by control of the wheel speed difference of an axle. It is applicable for vehicles with front-wheel or rear-wheel drive regarding electronically controlled limited-slip differentials and individually controllable brake actuators. The wheel dynamics were transformed in the sense of degrees of freedom which eliminated the coupling between actuator torques and wheel speeds. Control design was performed with input-output linearization. The scope of application of the existing Lyapunov function was extended to zero dynamics regarding different road frictions and wheel loads for the left and right wheel. The approach was evaluated in a test vehicle and improved the overall traction during accelerated cornering.

Future work could investigate the control performance in vehicles with individually controllable brake actuators or eLSD with higher actuator dynamics. Furthermore, the synthesis model (6) took only the cardan shaft as a torsion spring into account, while both drive shafts were modelled as a rigid connection. As mentioned in Reichensdörfer et al. (2019), it could be of great advantage to assume the drive shafts to be elastic as well. This would allow improved damping of torsional oscillations in the powertrain. Moreover, electric vehicles with single-wheel drive provide an additional possibility for torque vectoring. Further research could extend the approach to such electric motors or investigate the combination of multiple actuators regarding control allocation concepts for lateral torque distribution.

REFERENCES

Byrnes, C.I. and Isidori, A. (1989). New results and examples in nonlinear feedback stabilization. *Systems & Control Letters*, 12(5), 437–442.

Cheli, F., Giaramita, M., Pedrinelli, M., Sandoni, G., and Travaglio, G.C. (2005). A new control strategy for a semi-active differential (part I). *IFAC Proc.*, 38(1), 140–145.

Chen, J., Xu, G., Xu, K., and Li, W. (2012). Traction control for electric vehicles: A novel control scheme. In *2012 IEEE International Conference on Information and Automation*, 367–372.

de Castro, R.P., Santos Oliveira, H., Ricardo Soares, J., Cerqueira, N.M., and Araujo, R.E. (2007). A new FPGA based control system for electrical propulsion with electronic differential. In *2007 European Conference on Power Electronics and Applications*, 1–10.

Gilbert, G.T. (1991). Positive Definite Matrices and Sylvester's Criterion. *The Am. Math. Mon.*, 98(1), 44–46.

Hancock, M.J., Williams, R.A., Fina, E., and Best, M.C. (2007). Yaw motion control via active differentials. *Trans. Inst. Meas. Control*, 29(2), 137–157.

Hosomi, K., Nagae, A., Yamamoto, S., Takahira, Y., Koizumi, M., and Ishikawa, T. (2000). Development of Active-Traction Control System. In SAE (ed.), *SAE 2000 Automotive Dynamics & Stability Conference*, SAE Technical Paper Series.

Isermann, R. (2006). *Fahrdynamik-Regelung*. Vieweg+Teubner Verlag, Wiesbaden, 1st edition.

Isidori, A. (1989). *Nonlinear control systems*. Springer, Berlin, 2nd edition.

Ivanov, V., Savitski, D., and Shyrokau, B. (2015). A survey of traction control and antilock braking systems of full electric vehicles with individually controlled electric motors. *IEEE Trans. Veh. Technol.*, 64(9), 3878–3896.

Ivanović, V., Deur, J., Herold, Z., Hancock, M., and Assadian, F. (2012). Modelling of electromechanically actuated active differential wet-clutch dynamics. *Proc. of the Institution of Mech. Engineers*, 226(4), 433–456.

Marino, R. and Scalzi, S. (2008). Integrated active front steering and semiactive rear differential control in rear wheel drive vehicles. *IFAC Proc.*, 41(2), 10732–10737.

Pacejka, H. (2012). *Tire and vehicle dynamics*. Elsevier, San Diego.

Piyabongkarn, D., Grogg, J., Yuan, Q., Lew, J., and Rajamani, R. (2006). Dynamic modeling of torque-biasing devices for vehicle yaw control. In *SAE Technical Paper*.

Reichensdörfer, E., Degel, W., Odenthal, D., and Wollherr, D. (2019). Nonlinear traction control design, stability analysis and experiments for vehicles with on-demand 4WD torque bias systems. In *58th Conference on Decision and Control*, 6669–6674.

Reichensdörfer, E., Odenthal, D., and Wollherr, D. (2018). On the Stability of Nonlinear Wheel-Slip Zero Dynamics in Traction Control Systems. *IEEE Transactions on Control Systems Technology*.

Reichensdörfer, E., Odenthal, D., and Wollherr, D. (2020). Engine-Based Input-Output Linearization for Traction Control Systems. Accepted to IFAC World Congress 2020.

Resta, F., Teuschl, G., Zanchetta, M., and Zorzutti, A. (2005). A new control strategy for a semi-active differential (part II). *IFAC Proceedings*, 38(1), 146–151.

Rittmannsberger, N. (1988). Antilock Braking System And Traction Control. In *International Congress on Transportation Electronics*, 195–202.

Rosenberger, M., Schindele, F., Koch, T., and Lienkamp, M. (2012). Analyse und aktive Dämpfung von Antriebsstrangschwingungen bei Elektrofahrzeugen während der ABS-Regelung. In *8. Tag des Fahrwerks*.

van Zanten, A.T., Erhardt, R., and Pfaff, G. (1995). VDC, the Vehicle Dynamics Control system of Bosch. In *SAE Technical Paper 950759*.

Vitols, K. and Galkin, I. (2012). Analysis of electronic differential for electric kart. In *15th International Power Electronics and Motion Control Conference*.

Zech, A., Eberl, T., and Müller, S. (2017). Analyse einer neuen kaskadierten Reglerstruktur für die Antriebsschlupfbegrenzung hochdynamischer Fahrzeugantriebe. In *VDI/VDE Fachtagung, Automatisiertes Fahren und vernetzte Mobilität*, 287–297. VDI-Verlag, Düsseldorf.

Zech, A., Eberl, T., Reichensdörfer, E., and Odenthal, D. (2018). Method for developing tire slip controllers regarding a new cascaded controller structure. In *14th Int. Symp. on Advanced Vehicle Control*, 302–308.